

1 **Increased Primary and Secondary H<sub>2</sub>SO<sub>4</sub> Showing the Opposing Roles in SOA**  
2 **Formation from Ethyl Methacrylate Ozonolysis**

3 Peng Zhang <sup>a, c, #</sup>, Tianzeng Chen <sup>a, c, #</sup>, Jun Liu <sup>a, c</sup>, Guangyan Xu <sup>a, c</sup>, Qingxin Ma <sup>a, b, c \*</sup>,  
4 Biwu Chu <sup>a, b, c \*</sup>, Wanqi Sun<sup>d</sup>, and Hong He <sup>a, b, c</sup>

5 <sup>a</sup> State Key Joint Laboratory of Environment Simulation and Pollution Control,  
6 Research Center for Eco-Environmental Sciences, Chinese Academy of Sciences,  
7 Beijing 100085, China

8 <sup>b</sup> Center for Excellence in Regional Atmos. Environ., Institute of Urban Environment,  
9 Chinese Academy of Sciences, Xiamen 361021, China

10 <sup>c</sup> University of Chinese Academy of Sciences, Beijing 100049, China

11 <sup>d</sup> CMA Meteorological Observation Centre, Beijing, 100081, China

12 <sup>#</sup> These authors contributed equally to this work

13  
14  
15  
16  
17  
18  
19  
20  
21  
22  
23  
24  
25  
26  
27  
28  
29  
30

31 **Abstract**

32 Stressed plants and polymer production can emit many unsaturated volatile organic  
33 esters (UVOEs). However, secondary organic aerosol (SOA) formation of UVOEs  
34 remain unclear, especially under complex ambient conditions. In this study, we mainly  
35 investigated ethyl methacrylate (EM) ozonolysis. Results showed that a substantial  
36 increase in secondary H<sub>2</sub>SO<sub>4</sub> particles promoted SOA formation with increasing SO<sub>2</sub>.  
37 An important reason was that the homogeneous nucleation of more H<sub>2</sub>SO<sub>4</sub> at high SO<sub>2</sub>  
38 level provided greater surface area and volume for SOA condensation. However,  
39 increased primary H<sub>2</sub>SO<sub>4</sub> with seed acidity enhanced EM uptake, but reduced SOA  
40 formation. This was ascribed to the fact that the ozonolysis of more adsorbed EM was  
41 hampered with the formation of surface H<sub>2</sub>SO<sub>4</sub> at higher particle acidity. Moreover, the  
42 increase in secondary H<sub>2</sub>SO<sub>4</sub> particle via homogeneous nucleation favored to the  
43 oligomerization of oxidation products, whereas the increasing of primary H<sub>2</sub>SO<sub>4</sub> with  
44 acidity in the presence of seed tended to promote the functionalization conversion  
45 products. This study indicated that the role of increased H<sub>2</sub>SO<sub>4</sub> to EM-derived SOA  
46 maybe not the same under different ambient conditions, which helps to advance our  
47 understanding of the complicated roles of H<sub>2</sub>SO<sub>4</sub> in the formation of EM-derived SOA.

48  
49  
50  
51  
52  
53  
54  
55  
56  
57  
58  
59  
60  
61  
62  
63  
64  
65

## 66 **1. Introduction**

67 Unsaturated volatile organic esters (UVOEs) are oxygenated volatile organic  
68 compounds (OVOCs) with many large-scale commercial uses. They are not only used  
69 as potential replacements of traditional solvents and additive in diesel fuels but are  
70 widely used in the production of polymers and resins (Colomer et al., 2013; Taccone et  
71 al., 2016; Teruel et al., 2016; Wang et al., 2010). Thus, the production, processing,  
72 storage, and disposal of industrial products all contribute to UVOE emissions. In  
73 addition, emissions of green leaf volatiles (GLVs), a class of wound-induced OVOCs,  
74 also contribute to UVOEs in the atmosphere (Arey et al., 1991; Blanco et al., 2014;  
75 Hamilton et al., 2009; Konig et al., 1995). Once emitted into the atmosphere, these  
76 UVOEs quickly undergo complex chemical reactions with OH radicals and ozone in  
77 sunlight (Bernard et al., 2010; Blanco et al., 2010; Sun et al., 2015), NO<sub>3</sub> radicals during  
78 night-time (Salgado et al., 2011; Wang et al., 2010), and Cl atoms in certain  
79 environments (Blanco et al., 2010; Rivela et al., 2018). OH-initiated oxidation of GLVs,  
80 including *cis*-3-hexenylacetate (CHA) to secondary organic aerosol (SOA), is estimated  
81 to contribute 1–5 TgC/y, with up to a third of that from isoprene (Hamilton et al., 2009).  
82 In addition, CHA-derived SOA is a more efficient absorber (between 190 and 900 nm)  
83 than other OVOCs (such as *cis*-3-hexenol) due to the high proportion of carbonyl-  
84 containing species (Harvey et al., 2016). Thus, UVOEs can be considered as a class of  
85 potential SOA precursors. Further investigations on UVOE-derived SOA under  
86 complex ambient conditions will help to better understand their contribution to ambient  
87 aerosol.

88 Recent studies ascertained that the presence of SO<sub>2</sub> and sulfate seed particles all  
89 have a significant impact on the yield, composition, and formation mechanism of SOA  
90 (Han et al., 2016; Kristensen et al., 2014; Wong et al., 2015; Zhang et al., 2019). For  
91 example, an increase in SO<sub>2</sub> can enhance SOA production due to the formation of more  
92 sulfates and the enhanced acid-catalysis role during the atmospheric oxidation of  
93 various VOCs (Chu et al., 2016; Lin et al., 2013; Zhao et al., 2018). In the presence of  
94 alone seed particles, however, increased particle acidity will not always enhance SOA

95 formation and may have a negligible effect on the SOA formation(Han et al., 2016;  
96 Kristensen et al., 2014; Riva et al., 2016; Surratt et al., 2010; Wong et al., 2015; Zhang  
97 et al., 2019). Furthermore, it is worth noting that several studies have indicated that an  
98 increase in SO<sub>2</sub> can promote the average oxidation state (OS<sub>c</sub>) of SOA due to  
99 organosulfate formation(Liu et al., 2019a; Shu et al., 2018; Zhang et al., 2019). Whereas  
100 other studies have suggested that an increase SO<sub>2</sub> can have a suppression effect on SOA  
101 OS<sub>c</sub> (Friedman et al., 2016). Similarly, the effect of increased aerosol acidity on SOA  
102 OS<sub>c</sub> depends on the contribution of functionalization and oligomerization reactions to  
103 SOA composition as increased aerosol acidity can promote these reactions (Shu et al.,  
104 2018). This implies that the roles of increased sulfate particles and particle acidity in  
105 SOA production and composition are very complicated and need to be further studied.

106 Methacrylate was one of the main effluents in the class of UVOEs. Just in China,  
107 the net import of methacrylate has up to about 930 thousand tons in 2019. It was worth  
108 noting that ethyl methacrylate, one of methacrylate, has been widely detected in  
109 ambient air due to the wide variety of sources and high volatility (Pankow et al., 2003).  
110 Moreover, some exposure measurement studies indicated that the concentration of ethyl  
111 methacrylate was up to 31-108 μg m<sup>-3</sup> in the salons working air, which was notably  
112 higher than other methacrylate (Henriks-Eckerman and Korva, 2012). Thus, we used  
113 ethyl methacrylate (EM) as an UVOE proxy to investigate the effects of different SO<sub>2</sub>  
114 levels and seed particle acidity on the formation and evolution of EM-derived SOA in  
115 this work. This work will help to better understanding the formation of EM-derived  
116 SOA under complex conditions.

117

## 118 **2 Materials and methods**

119 Multiple EM ozonolysis experiments were conducted in a 30-m<sup>3</sup> cuboid Teflon smog  
120 chamber (L × W × H = 3.0 × 2.5 × 4.0 m) under 298 K temperature and atmospheric  
121 pressure. Experimental conditions are summarized in Table S1. The chamber operation,  
122 analytical techniques, and experimental procedures are described in detail elsewhere  
123 (Chen et al., 2019b). Only a brief description on the specific procedures relevant to this

124 work is presented here.

125 Prior to each experiment, the chamber was first inflated using purified and dry zero  
126 air with a flow rate of  $120 \text{ L min}^{-1}$  for 10 min, subsequently air pump began to run for  
127 5 min. The stainless-steel fan installed at the bottom of chamber was kept to run during  
128 the whole cleaning process. Prior to each experiment, Teflon chamber was repeatedly  
129 and circularly cleaned by purified and dry zero air using above method for about 24 h  
130 until almost no NO<sub>x</sub> could be detected or the particle number concentration was  $< 30$   
131  $\text{cm}^{-3}$ . The cleaning procedure of chamber was consistent with that described in our  
132 previous studies (Chen et al., 2019a; Liu et al., 2019a). The O<sub>3</sub> (generated by passing 4  
133  $\text{L min}^{-1}$  dry zero air over two UV photochemical tubes (40-cm length and 4-cm inter-  
134 diameter)), SO<sub>2</sub> (520 ppm in N<sub>2</sub>, Beijing Huayuan, China), and CO (0.05% in N<sub>2</sub>,  
135 Beijing Huayuan, China) were added into the chamber in sequence. EM were first  
136 added into a stainless-steel tee at 80 °C and subsequently flushed into the chamber by  
137 zero gas with the flowrate of  $20 \text{ L min}^{-1}$ . We applied CO to decrease the effect of OH  
138 radical reaction via scavenging of OH radicals. The EM (98% purity, Sigma-Aldrich,  
139 USA) was added to the chamber by injection of a known volume into a heated three-  
140 way tube (80 °C) and flushed into the chamber by dry zero air. A stainless-steel fan is  
141 used to ensure homogeneous mixing of reactants.

142 To minimize losses in the sampling line, various monitoring instruments  
143 surrounded and are next to the smog chamber. The length of sampling pipes of various  
144 monitoring instruments ranged from 0.5-1.0 m. A scanning mobility particle sizer  
145 (SMPS, TSI, Inc.), consisting of differential mobility analyzer (DMA; model 3082),  
146 condensation particle counter (CPC; model 1720), and Po210 bipolar neutralizer, was  
147 applied to measure number size distribution. Total particle number and mass  
148 concentrations were calculated assuming a uniform density for aerosol particles of  $1.4$   
149  $\text{g cm}^{-3}$  (Liu et al., 2019b; Chen et al., 2019b). The sheath flow and aerosol flow in the  
150 SMPS were set to  $3.0$  and  $0.3 \text{ L min}^{-1}$ , respectively. The SMPS results were further  
151 corrected via the wall loss rate of (NH<sub>4</sub>)<sub>2</sub>SO<sub>4</sub> particles and the correction magnitude is  
152 about 10% in 5 h-reaction (Figure S1). The desorption or off-gassing of organic gaseous

153 products and  $\text{NH}_3$  from chamber wall could be absorbed by seed particles to some  
154 extent during introducing seed particles. However, the influence of these particulate  
155 species to newly produced secondary particles could be ignorable based on the  
156 comparison of their concentrations (Figure S2).

157 Based on the different characterized fragments, both mass concentration and  
158 evolution of the different chemical compositions of aerosol particles were  
159 simultaneously measured online using High-Resolution Time-of-Flight Aerosol Mass  
160 Spectrometric Analysis (HR-ToF-AMS; Aerodyne Research Inc., USA). The AMS  
161 working principles and modes of operation are explained in detail elsewhere. According  
162 to standard protocols, the inlet flow rate, ionization efficiency (IE), and particle sizing  
163 were calibrated using size-selected pure ammonium nitrate (AN) particles (Drewnick  
164 et al., 2005). The HR-ToF-AMS analysis toolkit SQUIRREL 1.57I/PIKA v1.16I in Igor  
165 Pro v6.37 was employed to process and analyze the experimental data obtained by the  
166 HR-ToF-AMS. To reduce the sampling errors resulting from calibrating HR-TOF-  
167 AMS before each experiment, the HR-ToF-AMS results were further corrected using  
168 mass concentration derived from the SMPS as per Gordon et al (Gordon et al., 2014).  
169 A series of gas analyzers from Thermo Scientific (USA) were used to monitor the  
170 evolution of  $\text{SO}_2$  (model 43i),  $\text{CO}$  (model 48i), and  $\text{O}_3$  (model 49i) concentrations as a  
171 function of reaction time. Some recent studies indicated that higher  $\text{CO}$  levels were  
172 found to significantly change the chemical composition of SOA relative to low  $\text{CO}$  level  
173 (Zhang et al., 2020; McFiggans et al., 2019). Thus, about 36-38 ppm  $\text{CO}$  was added in  
174 the chamber to exclude  $\text{OH}$  radical influence during each experiment. Moreover, to  
175 make sure results reliable and rule out potential artifacts including the adding sequence  
176 of  $\text{CO}$ ,  $\text{O}_3$ , and  $\text{SO}_2$  during experimental preparation and the injection process of EM,  
177 parallel experiments (twice experiments at the same experimental conditions) under  
178 selected experimental conditions (135 ppb  $\text{SO}_2$  and in the presence of AS seeds,  
179 respectively) were conducted (Figure S3 and S4).

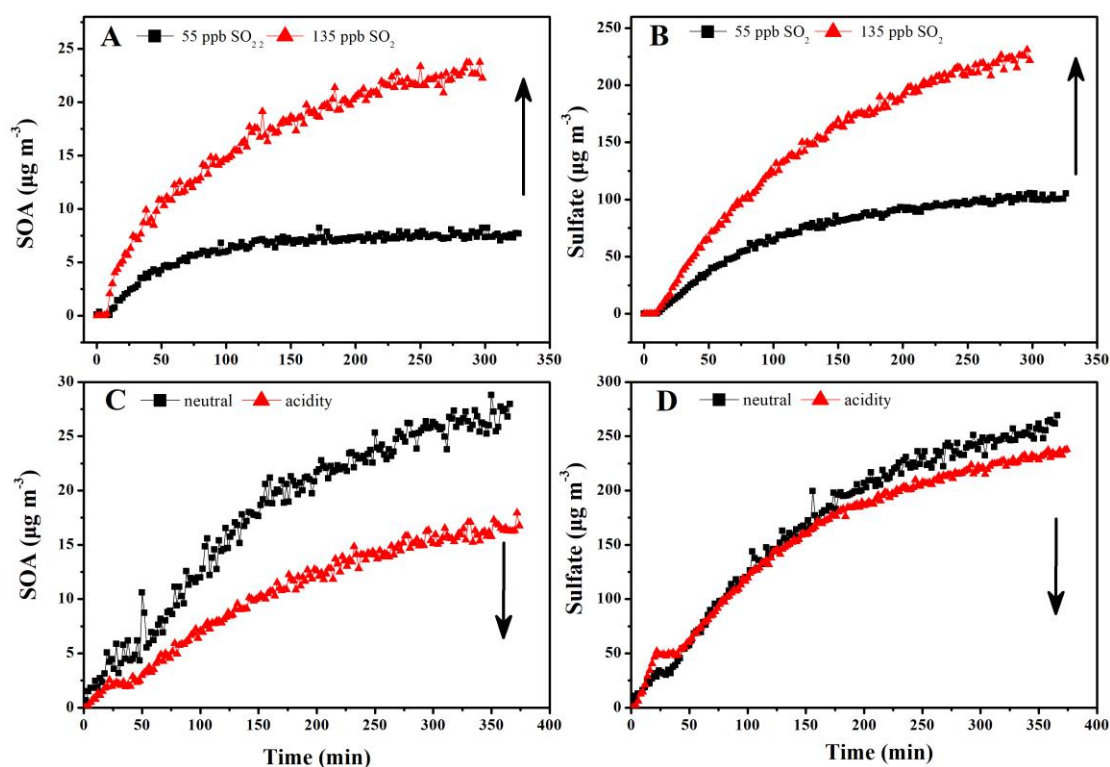
180

### 181 **3. Results and discussion**

### 182 **3.1. Overview of EM-derived SOA Formation with and without Seed Particles**

183 We first investigated the ozonolysis of alone EM. As shown in Figure S5, the  
184 ozonolysis of alone EM could not produce SOA in the absence of seed and SO<sub>2</sub>.  
185 Similarly, the increased particle acidity did not promote SOA formation during the  
186 ozonolysis of alone EM in the absence of SO<sub>2</sub> (Figure S6 and S7). Thus, this study  
187 mainly focused on EM ozonolysis in the presence of SO<sub>2</sub>. Secondary particle formation  
188 from EM ozonolysis with different SO<sub>2</sub> levels was first investigated in the absence of  
189 seed particles. As shown in Figure 1, SOA and sulfate were significantly produced once  
190 EM was introduced into the reaction chamber. Moreover, both SOA and sulfate  
191 formation were markedly enhanced with the increase in initial SO<sub>2</sub> concentration  
192 (Figure 1A and B). This indicated that EM-derived SOA formation was closely related  
193 to sulfate formation compared with that the ozonolysis of alone EM. Subsequently, EM  
194 ozonolysis with the same level of SO<sub>2</sub> (132-138 ppb) was also conducted in the  
195 presence of seed particles with different acidity (neutral and acidic). Two different  
196 solutions, including AS (0.02 mol L<sup>-1</sup>) and AS + H<sub>2</sub>SO<sub>4</sub> (0.02 + 0.04 mol L<sup>-1</sup>), were  
197 nebulized into the chamber, respectively, to provide the corresponding seed aerosol for  
198 acidity experiments. The initial seed concentrations have been added in the Table S1.  
199 Interestingly, with the increase of seed acidity, the maximum mass concentrations of  
200 SOA and sulfate decreased from 19.1 to 12.9 μg m<sup>-3</sup> (Figure 1C) and 192.6 to 169.7 μg  
201 m<sup>-3</sup> (Figure 1D), respectively. This indicated that increased particle acidity reduced  
202 secondary particle formation in the presence of SO<sub>2</sub>, which was inconsistent with the  
203 enhancement effect of particle acidity via acid-catalysis on SOA formation during  
204 alkene photooxidation (such as isoprene, isoprene epoxydiols, and glyoxal) (Kristensen  
205 et al., 2014; Lin et al., 2012; Riva et al., 2016; Wong et al., 2015). In order to evaluate  
206 whether the effect is atmospherically relevant, these experiments of seed particle role  
207 were also conducted at higher RH (45-50% RH). As shown in Figure S8, it could be  
208 found that increased particle acidity also suppressed the formation of SOA and sulfate  
209 at higher RH. Thus, these results imply that the increase of primary H<sub>2</sub>SO<sub>4</sub> proportion  
210 with particle acidity in seed particles and the increase of secondary H<sub>2</sub>SO<sub>4</sub> particles

211 with SO<sub>2</sub> concentration exhibited the opposite role in EM-derived SOA formation. In  
 212 addition, the change in RH was found to have an impact on the formation of EM-  
 213 derived SOA and sulfate, consistent with our recent studies (Zhang et al., 2019; Zhang  
 214 et al., 2020). SOA concentration at 45% RH was reduced by a factor of 2 relative to that  
 215 at 10% RH in this work (Figure S9). The changes in both sulfate and SOA concentration  
 216 were attributed to the competitive reaction between SO<sub>2</sub> and H<sub>2</sub>O toward sCI. The  
 217 suppression of H<sub>2</sub>SO<sub>4</sub> concentration was attributed to the rapid consumption of sCI by  
 218 water and water dimer at high RH (42%). The suppression of SOA mass loading should  
 219 be ascribed to the formation of volatile organic peroxides at high RH.



220

221 **Figure 1.** Time-dependent growth curves of SOA (A) and sulfate (B) under different  
 222 initial concentrations of SO<sub>2</sub> in absence of seed particles; SOA (C) and sulfate (D) after  
 223 subtracting seeds in presence of neutral and acidic seed particles.

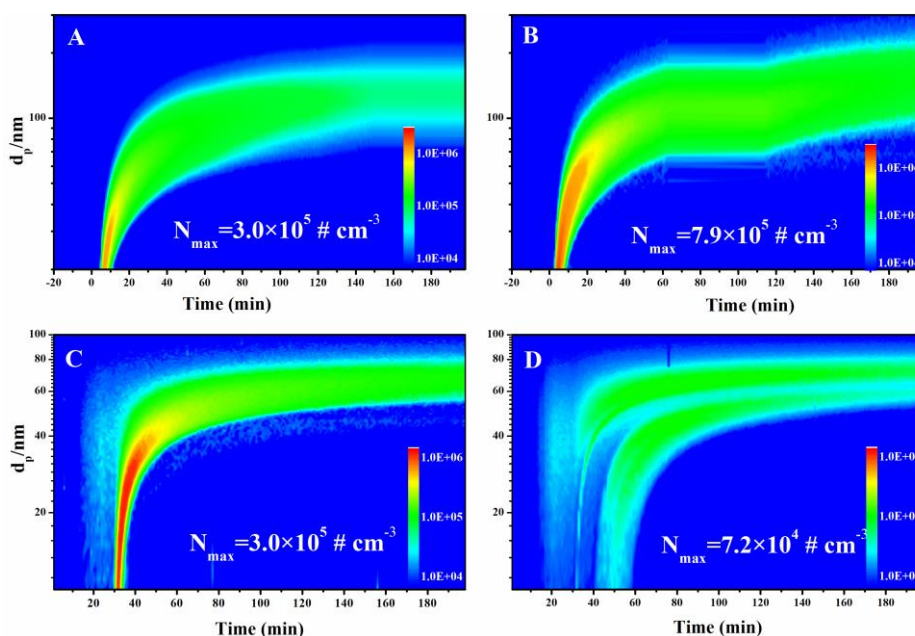
224 As shown in Figure 2, the size distributions of secondary particles under different  
 225 experimental conditions were also compared. The detected maximum particle  
 226 concentration (790 000 particle cm<sup>-3</sup>) under 135 ppb SO<sub>2</sub> was higher than that observed  
 227 under 55 ppb SO<sub>2</sub> (300 000 particle cm<sup>-3</sup>) in the absence of seed particles (Figure 2A  
 228 and B). Recent studies suggested that the reaction between SO<sub>2</sub> and stable Criegee



229 intermediates (sCI) dominated the formation of H<sub>2</sub>SO<sub>4</sub> particles and was enhanced with  
230 increased SO<sub>2</sub> concentration. An important reason for this is the rapid homogeneous  
231 nucleation of H<sub>2</sub>SO<sub>4</sub> not only can provide greater surface area and volume for the  
232 condensation of low-volatile products, but reduce the fraction of these semi-volatile  
233 species lost to the wall (Chu et al., 2016; Liu et al., 2017; Zhang et al., 2019; Zhang et  
234 al., 2014). The high PToF size of sulfate and surface concentration of fine particles at  
235 high SO<sub>2</sub> level supported above conclusion (Figure S10 and S11). In the presence of  
236 seed particles, we used similar average concentration (~25 000-30000 particles cm<sup>-3</sup>)  
237 under different acidities to reduce the disturbance of seed particle concentration (Figure  
238 2C and 2D). The mean size and surface concentration of acidified AS (AAS) was  
239 higher than AS (Figure S11B). Results showed ~300 000 newly produced particles cm<sup>-3</sup>  
240 <sup>3</sup> for neutral AS seeds (Figure 2C) and ~74 000 newly produced particles cm<sup>-3</sup> for  
241 acidified AS seeds (Figure 2D), respectively. The reduction of NPF in the presence of  
242 acidic particles most likely result from that acidic seed particles with high mean size  
243 and surface concentration promoted the condensation of gaseous nucleation species  
244 onto seed surface. However, this could not explain why both SOA and sulfate were all  
245 suppressed with the increase in particle acidity. Thus, one reasonable explanation is that  
246 acidic seed particles also enhanced EM uptake on the particle surface as well as  
247 promoting the condensation of nucleation species. As a result, the heterogeneous  
248 formation of fresher H<sub>2</sub>SO<sub>4</sub> on the surface of seed particles subsequently reduced SOA  
249 formation by hampering the ozonolysis of absorbed EM. To further supported this  
250 speculation, we first investigated the EM uptake on different using a gas mass  
251 spectrometer (QMS, GAM 200, Bremen, Germany). As shown in Figure S12, the  
252 increase in H<sub>2</sub>SO<sub>4</sub> concentration indeed promoted the uptake of EM on seed particle  
253 with the increase of acidity. To further verify the presence of SO<sub>2</sub> could hamper the  
254 ozonolysis of adsorbed EM due to surface H<sub>2</sub>SO<sub>4</sub> formation, we checked and compared  
255 the degradation of absorbed EM during its ozonolysis in the absence and presence of  
256 SO<sub>2</sub> using the in situ attenuated total internal reflection infrared (ATR-IR) spectra. As  
257 shown in Figure S13, it could be found that EM consumption in the presence of SO<sub>2</sub>

258 was slower than that in the absence of SO<sub>2</sub>. This indicated that higher particle acidity  
259 indeed promoted EM uptake on the particle surface and the presence of SO<sub>2</sub> resulted in  
260 the residual of more adsorbed EM on particle surface.

261 In addition, as shown in Figure S5 and S6, the negligible change of SOA with  
262 acidity in the absence of SO<sub>2</sub> also supported that the reducing effect of increasing  
263 particle acidity on secondary particle formation was closely related to the formation of  
264 H<sub>2</sub>SO<sub>4</sub> particles in the presence of SO<sub>2</sub>. And some recent studies proved that the  
265 presence of inorganic acids HCl can may also be an effective scavenger of sCI, further  
266 suppressing the formation of low-volatility oligomers (SOA composition) (Zhao et al.,  
267 2015). The reaction between sCI and HNO<sub>3</sub> or HCl in particularly was likely to be an  
268 important sink of sCI in polluted urban areas under dry conditions (Foreman et al.,  
269 2016). Thus, we speculated that the surface secondary reactions between sCI and H<sub>2</sub>SO<sub>4</sub>  
270 under acidity condition may also suppress the formation of low-volatility oligomers via  
271 affecting the sCI lifetime like HCl or HNO<sub>3</sub>. Taken together, these results imply that  
272 the SOA formation under different SO<sub>2</sub> levels and different particle acidities may be  
273 closely related to the homogeneous or heterogeneous formation of H<sub>2</sub>SO<sub>4</sub>.



274

275 **Figure 2.** Size distribution of secondary aerosol as a function of time at 55 ppb SO<sub>2</sub> (A)

276 and 135 ppb SO<sub>2</sub> (B) and under AS seed particle (C) and Acidic AAS seed particle (D).

277

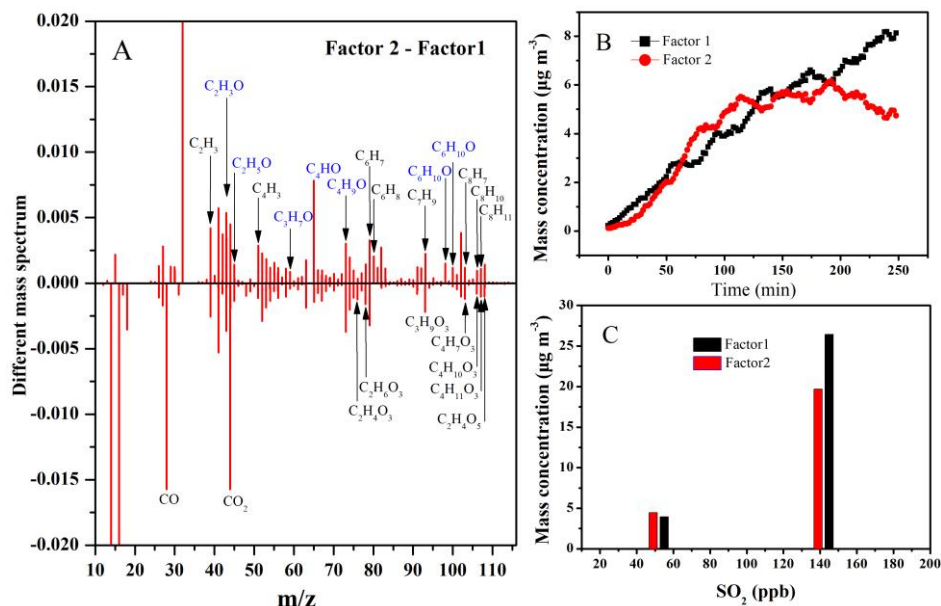
## 278 **3.2. Chemical Interpretation and Elemental Analysis of SOA**

279 Recent studies have suggested that a higher proportion of H<sub>2</sub>SO<sub>4</sub> in aerosol can  
280 result in greater formation of oligomers and high-oxygenated organic aerosol via  
281 acceleration of the acid-catalysis process (Iinuma et al., 2004; Kristensen et al., 2014;  
282 Liu et al., 2019a; Rodigast et al., 2017; Shu et al., 2018; Zhang et al., 2019). In order  
283 to make clear whether the homogeneous or heterogeneous formation of H<sub>2</sub>SO<sub>4</sub> could  
284 also affect SOA composition, we further analyze SOA composition and evolution based  
285 on positive matrix factorization (PMF) solution and Van Krevelen diagrams (Ulbrich  
286 et al., 2009; Zhang et al., 2005). The methodological of PMF analysis has been put into  
287 Supporting Information (Figure S14 and S15). The time series and mass spectra of each  
288 Factor after PMF analysis were applied to characterize the factor constitution and  
289 chemical conversion among factors (Ulbrich et al., 2009; Zhang et al., 2005).

### 290 ***Positive matrix factorization (PMF) solution***

291 In the absence of seed particles, two factors were identified under different SO<sub>2</sub>  
292 concentrations. As shown in Figure 3A, the 43 (C<sub>2</sub>H<sub>3</sub>O<sup>+</sup>) higher signals (tracers for  
293 alcohols and aldehydes) and prominent fragmental peaks containing one-oxygen atom  
294 (i.e., C<sub>2</sub>H<sub>4</sub>O, C<sub>2</sub>H<sub>5</sub>O, C<sub>3</sub>H<sub>5</sub>O, C<sub>3</sub>H<sub>5</sub>O, C<sub>3</sub>H<sub>7</sub>O, C<sub>4</sub>HO, and C<sub>6</sub>H<sub>10</sub>O) observed in Factor  
295 2 implied that Factor 2 consisted of less-oxygenated organic aerosols. The 44 (CO<sub>2</sub><sup>+</sup>)  
296 higher signals, tracers for organic acids, and dominant peaks containing multi-oxygen  
297 atoms (i.e., C<sub>3</sub>H<sub>8</sub>O<sub>3</sub>, C<sub>3</sub>H<sub>9</sub>O<sub>3</sub>, and C<sub>4</sub>H<sub>10</sub>O<sub>3</sub>) observed in Factor 1 implied that Factor 1  
298 consisted of more-oxygenated organic aerosols. From the temporal variations in Figure  
299 3B, both Factor 1 and 2 continuously increased with reaction progress before 200 min.  
300 This implied that both Factors were simultaneously produced and SOA growth should  
301 be mainly attributed to the adsorption and condensation of both less oxidized species  
302 and more oxidized species on particle before 200 min. After 200 min, Factor 1  
303 continuously increased but Factor 2 decreased, suggesting that the chemical conversion  
304 of part of less-oxygenated species in Factor 2 to more-oxygenated products in Factor 1  
305 in the latter period of reaction. Moreover, the average elemental compositions of Factor  
306 1 and Factor 2 were estimated to be C<sub>2.29</sub>H<sub>3</sub>O<sub>0.53</sub>S<sub>0.01</sub> and C<sub>1.38</sub>H<sub>1.87</sub>O<sub>0.37</sub>S<sub>0.027</sub>,

307 respectively. Higher OS<sub>c</sub> of Factor 2 (-0.85) relative to that Factor 1 (-0.81) also  
 308 supported above conclusion. This also implied that the acid-catalyzed role could  
 309 promote the chemical conversion from Factor 2 to Factor 1 when the H<sub>2</sub>SO<sub>4</sub> proportion  
 310 (acidity) in the particle-phase reached a certain concentration (Liu et al., 2019a;  
 311 Offenberg et al., 2009). The evolution of org 43 and org 44 fragments, representing the  
 312 characterized fragment of low-and high-oxidized species, further supported above  
 313 conclusion (Figure S16). As shown in Figure 3C, the maximum production of both  
 314 Factor 1 and Factor 2 increased with increasing SO<sub>2</sub>. One reasonable explanation is that  
 315 the formation of more H<sub>2</sub>SO<sub>4</sub> particles with increasing SO<sub>2</sub> provided a greater surface  
 316 area and volume for the simultaneous condensation of both less-oxygenated and more-  
 317 oxygenated organic products (Chu et al., 2016; Liu et al., 2017; Zhang et al., 2019).

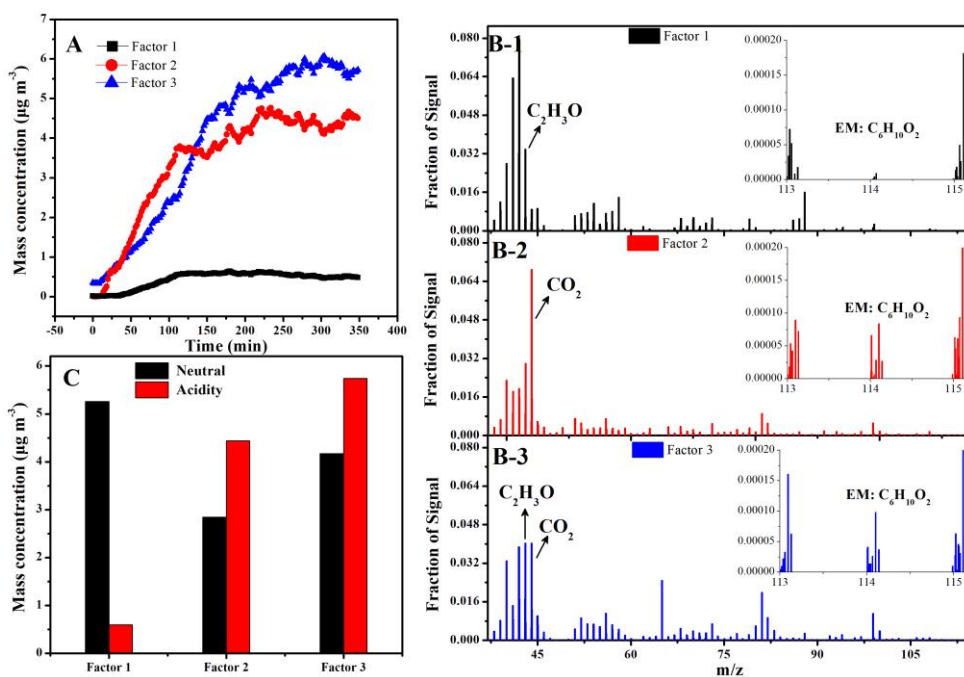


318  
 319 **Figure 3.** Two-factor solutions for PMF analyses of SOA under different SO<sub>2</sub>  
 320 concentrations: (A) Different mass spectra between two factors (Factor 2-Factor 1) at  
 321 135 ppb SO<sub>2</sub>; (B) Time series of factor concentrations; (C) Maximum concentration of  
 322 two factors at 55 ppb and 135 ppb SO<sub>2</sub>.

323 In the presence of seed particles, the chemical evolution of SOA components under  
 324 different acidity conditions was also compared based on PMF analysis. From the  
 325 temporal variations in Figure 4A, three factors were identified and almost  
 326 simultaneously increased. Based on the mass spectra of the three factors (Figure 4B),

327 the fragments containing less-oxygenated species in Factor 1 (such as typical fragment  
328  $C_2H_3O^+$  ( $m/z$  43)) were more abundant than in Factor 2. In contrast, the fragments  
329 containing more-oxygenated species in Factor 2 (such as typical fragment  $CO_2^+$  ( $m/z$   
330 44)) were more abundant than in Factor 1. Thus, Factor 1 and 2 were tentatively  
331 assigned to less-oxygenated and more-oxygenated organic aerosols, respectively. This  
332 proved that the increase in particle acidity simultaneously promoted the formation of  
333 both less and more-oxygenated species, similar to that in the  $SO_2$  experiments. However,  
334 it is worth noting that higher acidity significantly promoted the chemical conversion of  
335 less-oxygenated species (Factor 1) to more-oxygenated species (Factor 2) via  
336 functionalization based on the comparison between the neutral and acidic seed particles  
337 (Figure 4C). As shown in Figure 4B, the ion at  $m/z$  114 ( $C_6H_{10}O_2$ ) was assigned to  
338 precursor-related ions. The highest ion signal fraction ( $m/z$  114) in Factor 3 and the  
339 similar mass spectrum between EM and Factor 3 in Figure S13 implied that Factor 3  
340 represented precursor-related species (Figure 4C).

341 Based on the comparison of Factors between seed experiments and  $SO_2$ , it should  
342 be noted that Factor 1 and Factor 2 in the seed experiments differed from that in the  
343  $SO_2$  experiment. For  $SO_2$  experiments, acidity appeared to convert Factor 2 to Factor  
344 1 after 200 minutes, but in seed experiments, the more  $H_2SO_4$  caused the formation of  
345 more Factor 2 and less Factor 1. Thus, we concluded that, for the same Factor in two  
346 types of experiments, the corresponding composition should be different each other.  
347 One possible explanation for this was that the increase in primary and secondary  $H_2SO_4$   
348 particles could also affect SOA composition to some extent, such as via changing the  
349 reaction pathway of sCI.



350

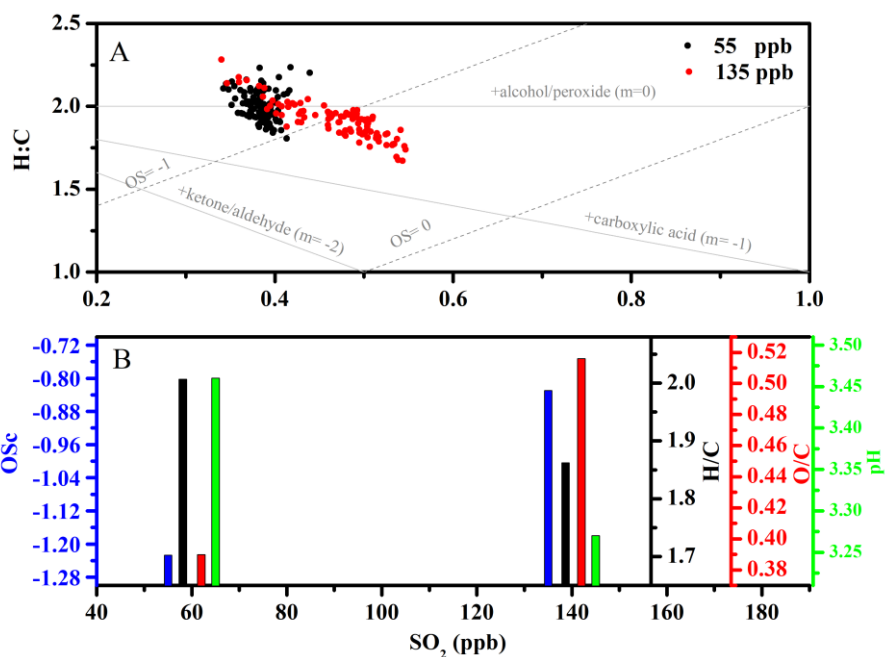
351 **Figure 4.** Three-factor solutions for PMF analyses of SOA under different seed  
 352 particles: (A) Time series of factor concentrations under acidic AAS; (B) Mass spectra  
 353 of three factors; (C) Comparison of maximum concentration of two factors under  
 354 neutral AS (black) and acidic AAS (red).

355 *Elemental analysis in Van Krevelen diagrams*

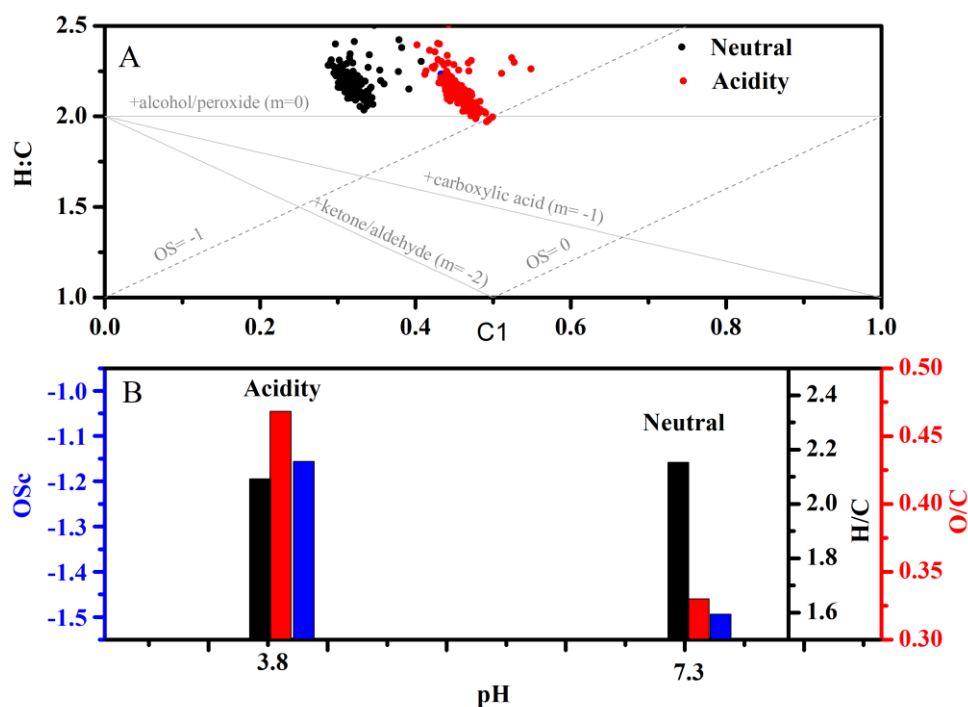
356 The rate at which the H/C ratio changes with the O/C ratio in Van Krevelen  
 357 diagrams can provide new information about the functional groups formed during  
 358 oxidation (Chen et al., 2011; Lambe et al., 2012; Lambe et al., 2011; Li et al., 2019).  
 359 As shown in Figure 5A and 6A, the average (H/C)/(O/C) slopes under different  
 360 experimental conditions all approached -2. A slope of -2 is due to the formation of  
 361 carbonyl species (Ng et al., 2011). This is consistent with the acknowledged reaction  
 362 mechanism of alkene ozonolysis in the presence of SO<sub>2</sub>, in which many carbonyl  
 363 species and H<sub>2</sub>SO<sub>4</sub> particles are produced (Newland et al., 2015a; Newland et al., 2015b;  
 364 Sadezky et al., 2006; Sadezky et al., 2008). To verify whether increased OS<sub>c</sub> was related  
 365 to particle pH, particle pH was estimated using the E-AIM model (Model II: H<sup>+</sup> – NH<sub>4</sub><sup>+</sup>  
 366 – SO<sub>4</sub><sup>2-</sup> – NO<sub>3</sub><sup>-</sup> – H<sub>2</sub>O) when secondary particle formation peaked under different SO<sub>2</sub>  
 367 concentrations (Hennigan et al., 2015; Peng et al., 2019). Since no organics are  
 368 considered in Model II, there was an inherent assumption here that the acidity and the

369 water uptake was dominated by the inorganic ions. From Figure 5B, the acidity for  
370 nucleated H<sub>2</sub>SO<sub>4</sub> particles (pH) under different SO<sub>2</sub> concentration have been estimated  
371 to be 3.27 and 3.46, respectively. The acidities for AS and AAS (pH) have been  
372 estimated to 7.3 and 4.1, respectively. The averaged oxidation state (OS<sub>c</sub>) of SOA  
373 increased with decreasing particulate pH in the absence of seeds. Similar trend was also  
374 observed in the presence of seed particles (Figure 6B). This indicated that increased  
375 OS<sub>c</sub> was closely related to increased particles acidity either in the presence or absence  
376 of seed particles. These results also indicated that both functionalization and  
377 oligomerization associated with carbonyls groups dominate the formation of EM-  
378 derived SOA. Moreover, it is worth noting that O/C increased when H/C decreased with  
379 increased particle acidity in the absence of seed particles. In contrast, the O/C ratio  
380 increased but the H/C ratio basically remained stable with increased particle acidity in  
381 the presence of seed particles. These results implied that increased particle acidity  
382 tended to promote the formation of more highly oxidized products via oligomerization  
383 in the absence of seed particles and tended to promote the formation of more highly  
384 oxidized products via functionalization in the presence of seed particles (Darer et al.,  
385 2011; Shu et al., 2018; Zhang et al., 2019). However, the promoting contribution of  
386 SOA functionalization conversion of total SOA could be ignored compared with the  
387 reducing effect of acidic particles. Some studies showed that increased OS<sub>c</sub> was closely  
388 related to the formation of organosulfate (Liu et al., 2019a; Shu et al., 2018; Zhang et  
389 al., 2019). To verify the organosulfate formation, the sulfate fragments along with S/C  
390 ratio between AS and AAS experiments were also compared. As shown in Figure S17,  
391 the similar S/C ratio and sulfate fragments distribution between neutral and acidic seed  
392 experiments excluded the contribution of organosulfate formation to increased OS<sub>c</sub>  
393 (Chen et al., 2019c).

394



395  
 396 **Figure 5.** Van Krevelen diagrams of elemental ratios under different initial  
 397 concentrations of  $\text{SO}_2$  (A); change in H/C ratio (black), O/C ratio (red),  $\text{OS}_c$  (blue), and  
 398 particle pH (green) as a function of initial  $\text{SO}_2$  concentration (B).

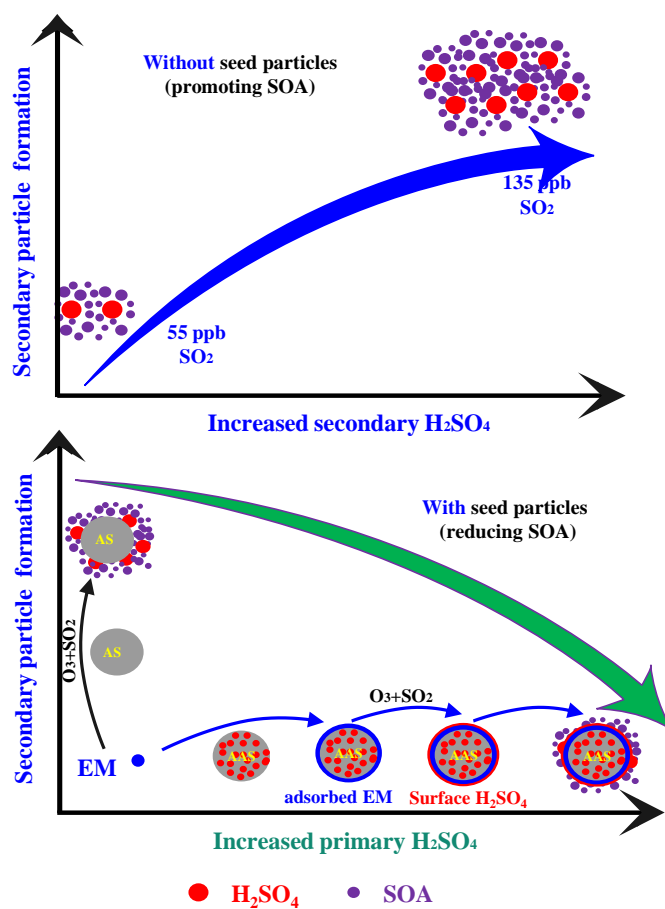


399  
 400 **Figure 6.** Van Krevelen diagrams of elemental ratios under different seed particle  
 401 acidity (A); change in H/C ratio (black), O/C ratio (red), and  $\text{OS}_c$  (blue) with particle  
 402 acidity (B).

403 Taken together, in the absence of seed particles, the homogeneous formation of



404 more H<sub>2</sub>SO<sub>4</sub> particles not only promoted the quick condensation of less- and more-  
 405 oxygenated products and subsequent SOA formation via providing a greater surface  
 406 area and volume, but enhanced the oligomerization process (Figure 7). In the presence  
 407 of seed particles, the presence of more primary H<sub>2</sub>SO<sub>4</sub> in seed particle enhanced EM  
 408 uptake and functionalization process, but reduced SOA production due to the formation  
 409 of surface H<sub>2</sub>SO<sub>4</sub>. This further indicated that the increase in primary and secondary  
 410 H<sub>2</sub>SO<sub>4</sub> particles could significantly affect SOA formation and composition.



411

412

**Figure 7.** Proposed the role of H<sub>2</sub>SO<sub>4</sub> formation on EM-derived SOA

413

### 414 3.3. Reaction Mechanism of EM Ozonolysis

415

416

417

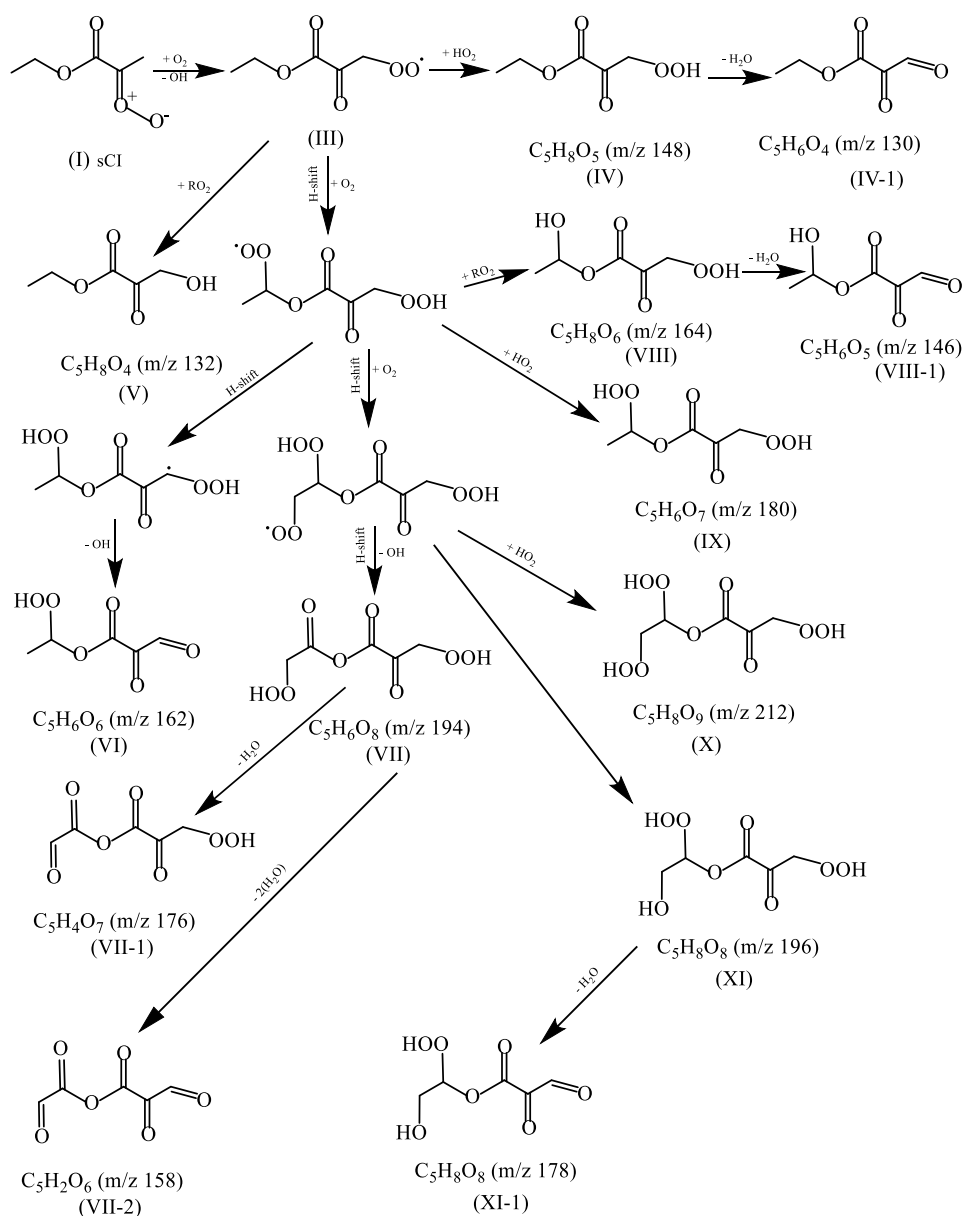
418

419

In order to make clear the formation mechanism of EM-derived SOA, the evolutions of some molecular ion peaks have been checked in detail. As shown in Figure S18, the increase of their mass concentrations with reaction time indicated that these molecular ions peaks with m/z 116, 130, 132, 140, 146, 148, 158, 162, 164, 176, 178, 180, 194, 196, and 212 should be the major ozonolysis products. Based on the

420 previously reported mechanism of alkene ozonolysis, the mechanism of EM ozonolysis  
421 has been proposed in Scheme S1 (Jain et al., 2014; Vereecken and Francisco, 2012).  
422 Briefly, oxidation of EM is initiated by addition of ozone across the double bond  
423 resulting in a primary ozonide. The primary ozonide will produce two products  
424 (formaldehyde and ketone ester) and two sCIs (sCI-1 and sCI-2). Based on the initial  
425 carbonyl and sCI products (Scheme S1), it could be found that the saturated ketone ester  
426 couldn't be further oxidized by O<sub>3</sub> and formaldehyde was the terminate products of sCI-  
427 2 reaction. Thus, these major oxidation products observed in Figure S18 should come  
428 from the further reaction of sCI-1. The mechanism of EM ozonolysis was proposed  
429 based on previous studies (Bianchi et al., 2019; Jokinen et al., 2014; Newland et al.,  
430 2018). Some highly oxidized multifunctional compounds could be produced via the H-  
431 shift process including 1,7- and 1,8-H shift (Kurten et al., 2015; Mackenzie-Rae et al.,  
432 2018). Thus, we concluded that the H-shift followed by autoxidation could be proposed  
433 to be a formation pathway of highly oxidized multifunctional compounds.

434 Proposed reaction mechanism of sCI-1 was also shown in Scheme 1. These sCI-1 could  
435 first convert to alkoxy radical (III) by losing OH group and O<sub>2</sub> addition. Then alkoxy  
436 radical with an additional oxygen atom not only could further react with RO<sub>2</sub> to form  
437 alcohols (V), but also react with HO<sub>2</sub> to form hydroperoxide product (IV). Moreover,  
438 the intramolecular H-shift reaction may also compete with its bimolecular reaction with  
439 HO<sub>2</sub> and other RO<sub>2</sub> radicals due to relatively weak C-H bonds in the molecule (Crouse  
440 et al., 2013; Jokinen et al., 2014; Shu et al., 2018). Similarly, newly produced alkoxy  
441 radical will continually and repeatedly react with HO<sub>2</sub>, RO<sub>2</sub>, and undergo its  
442 intramolecular H-shift to form the higher oxidized alcohols, carbonyls, and  
443 hydroperoxide product. The formation of these higher oxidized alcohols, carbonyls, and  
444 hydroperoxide product might help to explain or give insight to the increased oxidation  
445 state (OS<sub>c</sub>) of the aerosol.



446

447 **Scheme 1.** Proposed mechanism for EM ozonolysis in the presence of AS particles

448

#### 449 4. Conclusion

450 Some exposure measurement studies indicated that the concentration of ethyl  
 451 methacrylate was notably higher than other methacrylate in the salons working air. The  
 452 frequently exposure of methacrylate for a long time can trigger asthma or allergic  
 453 contact dermatitis. Thus, the wide variety of sources and high volatility and toxicity of  
 454 make EM a potential important source of environmental concern in the atmosphere. In  
 455 China,  $O_3$  pollution is gradually becoming serious environmental problem with the

456 decrease in PM<sub>2.5</sub> concentration recent years. sCI, as a key reactive intermediate in  
457 alkene ozonolysis, has been frequently reported to exhibit high oxidation capability in  
458 the conversion of SO<sub>2</sub> and NO<sub>2</sub> to secondary particles (Newland et al., 2018). Thus,  
459 investigating the ozonolysis of EM under complex condition help to evaluate their  
460 potential contribution to haze formation.

461 In this work, we investigated and compared the formation of secondary particles  
462 from EM ozonolysis under complex ambient condition. Results showed that a  
463 substantial increase in secondary H<sub>2</sub>SO<sub>4</sub> particles promoted SOA formation with  
464 increasing SO<sub>2</sub>. In contrast, the increase in primary H<sub>2</sub>SO<sub>4</sub> proportion with seed acidity  
465 enhanced EM uptake but reduced SOA formation. To clarify the underlying causes, we  
466 analyzed the size distribution, chemical composition and evolution of SOA based on  
467 PMF solutions and Van Krevelen diagrams. In the absence of seed particles, the  
468 substantial increase in secondary H<sub>2</sub>SO<sub>4</sub> particles with SO<sub>2</sub> provided greater surface  
469 area and volume for further condensation of oxidation products. Moreover, enhanced  
470 oligomerization functionalization of carbonyl species with increased particle acidity  
471 also contributed to the increase in SOA in the absence of seed particles. However, in  
472 the presence of seed particles, the increase of primary H<sub>2</sub>SO<sub>4</sub> proportion in seed with  
473 acidity enhanced more EM uptake, but the direct heterogeneous formation of H<sub>2</sub>SO<sub>4</sub> on  
474 the particle surface, differing from the condensation or nucleation of gas-phase H<sub>2</sub>SO<sub>4</sub>,  
475 hampered the continuous heterogeneous ozonolysis of these adsorbed EM. Moreover,  
476 even though increased particles acidity also caused chemical conversion of SOA via  
477 functionalization, the contribution of the produced functionalized products to SOA  
478 could be ignored due to the limited change in overall SOA formation. These results  
479 indicated that the increase of primary and secondary H<sub>2</sub>SO<sub>4</sub> particle has the different  
480 effect on EM-derived SOA formation and its composition.

481 Taken together, our findings help to further understand the complicated effects of  
482 increased H<sub>2</sub>SO<sub>4</sub> components on SOA formation and composition during haze pollution.  
483 However, more quantitative investigation based on a proton transfer reaction time-of-  
484 flight mass spectrometry (PTR-TOFMS) and Nitrate ion chemical ionization mass

485 spectrometry (NO<sub>3</sub>-CIMS) would be very necessary to accurately evaluate the  
486 contribution of H<sub>2</sub>SO<sub>4</sub> particles to SOA formation (yield) and composition (molecule  
487 structure) in the future study. In addition to EM, many other unsaturated esters such as  
488 methyl methacrylate (MA), butyl methacrylate (BMA), and propyl methacrylate (PMA)  
489 are also frequently measured in the real atmosphere (Blanco et al., 2014; Ren et al.,  
490 2019). Thus, more researches are needed to investigate the secondary particles potential  
491 of these unsaturated esters, especially under complex ambient conditions, which will  
492 help to further effectively evaluate the potential contribution of their atmospheric  
493 oxidation process to secondary particle formation.

494

#### 495 **Corresponding Author and Author Contributions**

496 \* Phone: (+86)-010-62849508;

497 E-mail: qxma @rcees.ac.cn.

498 E-mail: bwchu @rcees.ac.cn.

499 PZ and TC designed and conducted this experiment, TC helped to analyze experimental  
500 data. JL, XG, and WS gave assistance in measurements. HH, QM and BC discussed the  
501 data results. PZ wrote the paper with input from all coauthors. All authors contributed  
502 to the final paper.

503

#### 504 **Notes**

505 The authors declare no competing financial interests.

506

#### 507 **Acknowledgments**

508 This work was financially supported by the National Natural Science Foundation of  
509 China (21976098, 22006152, 41605100, 41705134, 21876185, 91744205, and  
510 41877304).

511

#### 512 **References**

513 Arey, J., Winer, A. M., Atkinson, R., Aschmann, S. M., Long, W. D., and Morrison, C. L.: The Emission

514 of (Z)-3-Hexen-1-ol, (Z)-3-Hexenylacetate and Other Oxygenated Hydrocarbons from Agricultural  
515 Plant-Species, *Atmos Environ a-Gen*, 25, 1063-1075, Doi 10.1016/0960-1686(91)90148-Z, 1991.

516 Bernard, F., Eyglunent, G., Daele, V., and Mellouki, A.: Kinetics and products of gas-phase reactions of  
517 ozone with methyl methacrylate, methyl acrylate, and ethyl acrylate, *J. Phys. Chem. A*, 114, 8376-8383,  
518 10.1021/jp104451v, 2010.

519 Bianchi, F., Kurten, T., Riva, M., Mohr, C., Rissanen, M. P., Roldin, P., Berndt, T., Crouse, J. D.,  
520 Wennberg, P. O., Mentel, T. F., Wildt, J., Junninen, H., Jokinen, T., Kulmala, M., Worsnop, D. R.,  
521 Thornton, J. A., Donahue, N., Kjaergaard, H. G., and Ehn, M.: Highly Oxygenated Organic Molecules  
522 (HOM) from Gas-Phase Autoxidation Involving Peroxy Radicals: A Key Contributor to Atmospheric  
523 Aerosol, *Chem. Rev.*, 119, 3472-3509, 10.1021/acs.chemrev.8b00395, 2019.

524 Blanco, M. B., Bejan, I., Barnes, I., Wiesen, P., and Teruel, M. A.: FTIR product distribution study of the  
525 Cl and OH initiated degradation of methyl acrylate at atmospheric pressure, *Environ. Sci. Technol.*, 44,  
526 7031-7036, 10.1021/es101831r, 2010.

527 Blanco, M. B., Bejan, I., Barnes, I., Wiesen, P., and Teruel, M. A.: Products and mechanism of the  
528 reactions of OH radicals and Cl atoms with methyl methacrylate ( $\text{CH}_2=\text{C}(\text{CH}_3)\text{C}(\text{O})\text{OCH}_3$ ) in the  
529 presence of NO<sub>x</sub>, *Environ. Sci. Technol.*, 48, 1692-1699, 10.1021/es404771d, 2014.

530 Chen, Q., Liu, Y., Donahue, N. M., Shilling, J. E., and Martin, S. T.: Particle-phase chemistry of  
531 secondary organic material: modeled compared to measured O:C and H:C elemental ratios provide  
532 constraints, *Environ. Sci. Technol.*, 45, 4763-4770, 10.1021/es104398s, 2011.

533 Chen, T. Z., Liu, Y. C., Liu, C. G., Liu, J., Chu, B. W., and He, H.: Important role of aromatic  
534 hydrocarbons in SOA formation from unburned gasoline vapor, *Atmos. Environ.*, 201, 101-109,  
535 10.1016/j.atmosenv.2019.01.001, 2019a.

536 Chen, T. Z., Liu, Y. C., Ma, Q. X., Chu, B. W., Zhang, P., Liu, C. G., Liu, J., and He, H.: Significant  
537 source of secondary aerosol: formation from gasoline evaporative emissions in the presence of SO<sub>2</sub> and  
538 NH<sub>3</sub>, *Atmos. Chem. Phys.*, 19, 8063-8081, 10.5194/acp-19-8063-2019, 2019b.

539 Chen, Y., Xu, L., Humphry, T., Hettiyadura, A. P. S., Ovadnevaite, J., Huang, S., Poulain, L., Schroder,  
540 J. C., Campuzano-Jost, P., Jimenez, J. L., Herrmann, H., O'Dowd, C., Stone, E. A., and Ng, N. L.:  
541 Response of the Aerodyne Aerosol Mass Spectrometer to Inorganic Sulfates and Organosulfur  
542 Compounds: Applications in Field and Laboratory Measurements, *Environ. Sci. Technol.*, 53, 5176-5186,

543 10.1021/acs.est.9b00884, 2019c.

544 Chu, B. W., Zhang, X., Liu, Y. C., He, H., Sun, Y., Jiang, J. K., Li, J. H., and Hao, J. M.: Synergetic  
545 formation of secondary inorganic and organic aerosol: effect of SO<sub>2</sub> and NH<sub>3</sub> on particle formation and  
546 growth, *Atmos. Chem. Phys.*, 16, 14219-14230, 10.5194/acp-16-14219-2016, 2016.

547 Colomer, J. P., Blanco, M. B., Penenory, A. B., Barnes, I., Wiesen, P., and Teruel, M. A.: FTIR gas-phase  
548 kinetic study on the reactions of OH radicals and Cl atoms with unsaturated esters: Methyl-3,3-dimethyl  
549 acrylate, (E)-ethyl tiglate and methyl-3-butenolate, *Atmos. Environ.*, 79, 546-552,  
550 10.1016/j.atmosenv.2013.07.009, 2013.

551 Crounse, J. D., Nielsen, L. B., Jorgensen, S., Kjaergaard, H. G., and Wennberg, P. O.: Autoxidation of  
552 Organic Compounds in the Atmosphere, *J. Phys. Chem. Lett.*, 4, 3513-3520, 10.1021/jz4019207, 2013.

553 Darer, A. I., Cole-Filipiak, N. C., O'Connor, A. E., and Elrod, M. J.: Formation and stability of  
554 atmospherically relevant isoprene-derived organosulfates and organonitrates, *Environ. Sci. Technol.*, 45,  
555 1895-1902, 10.1021/es103797z, 2011.

556 Drewnick, F., Hings, S. S., DeCarlo, P., Jayne, J. T., Gonin, M., Fuhrer, K., Weimer, S., Jimenez, J. L.,  
557 Demerjian, K. L., Borrmann, S., and Worsnop, D. R.: A new time-of-flight aerosol mass spectrometer  
558 (TOF-AMS) - Instrument description and first field deployment, *Aerosol Sci. Technol.*, 39, 637-658,  
559 10.1080/02786820500182040, 2005.

560 Foreman, E. S., Kapnas, K. M., and Murray, C.: Reactions between Criegee Intermediates and the  
561 Inorganic Acids HCl and HNO<sub>3</sub> : Kinetics and Atmospheric Implications, *Angew. Chem. Int. Ed. Engl.*,  
562 55, 10419-10422, 10.1002/anie.201604662, 2016.

563 Friedman, B., Brophy, P., Brune, W. H., and Farmer, D. K.: Anthropogenic Sulfur perturbations on  
564 biogenic oxidation: so<sub>2</sub> additions impact gas-phase oh oxidation products of alpha- and beta-pinene,  
565 *Environ. Sci. Technol.*, 50, 1269-1279, 10.1021/acs.est.5b05010, 2016.

566 Gordon, T. D., Presto, A. A., May, A. A., Nguyen, N. T., Lipsky, E. M., Donahue, N. M., Gutierrez, A.,  
567 Zhang, M., Maddox, C., Rieger, P., Chattopadhyay, S., Maldonado, H., Maricq, M. M., and Robinson, A.  
568 L.: Secondary organic aerosol formation exceeds primary particulate matter emissions for light-duty  
569 gasoline vehicles, *Atmos. Chem. Phys.*, 14, 4661-4678, 10.5194/acp-14-4661-2014, 2014.

570 Hamilton, J. F., Lewis, A. C., Carey, T. J., Wenger, J. C., Garcia, E. B. I., and Munoz, A.: Reactive  
571 oxidation products promote secondary organic aerosol formation from green leaf volatiles, *Atmos. Chem.*

572 Phys., 9, 3815-3823, 10.5194/acp-9-3815-2009, 2009.

573 Han, Y. M., Stroud, C. A., Liggio, J., and Li, S. M.: The effect of particle acidity on secondary organic  
574 aerosol formation from alpha-pinene photooxidation under atmospherically relevant conditions, Atmos.  
575 Chem. Phys., 16, 13929-13944, 10.5194/acp-16-13929-2016, 2016.

576 Harvey, R. M., Bateman, A. P., Jain, S., Li, Y. J., Martin, S., and Petrucci, G. A.: Optical Properties of  
577 Secondary Organic Aerosol from cis-3-Hexenol and cis-3-Hexenyl Acetate: Effect of Chemical  
578 Composition, Humidity, and Phase, Environ. Sci. Technol., 50, 4997-5006, 10.1021/acs.est.6b00625,  
579 2016.

580 Hennigan, C. J., Izumi, J., Sullivan, A. P., Weber, R. J., and Nenes, A.: A critical evaluation of proxy  
581 methods used to estimate the acidity of atmospheric particles, Atmos. Chem. Phys., 15, 2775-2790,  
582 10.5194/acp-15-2775-2015, 2015.

583 Henriks-Eckerman, M. L., and Korva, M.: Exposure to airborne methacrylates in nail salons, J. Occup.  
584 Environ. Hyg, 9, D146-150, 10.1080/15459624.2012.696023, 2012.

585 Inuma, Y., Boge, O., Gnauk, T., and Herrmann, H.: Aerosol-chamber study of the alpha-pinene/O<sub>3</sub>  
586 reaction: influence of particle acidity on aerosol yields and products, Atmos. Environ., 38, 761-773,  
587 10.1016/j.atmosenv.2003.10.015, 2004.

588 Jain, S., Zahardis, J., and Petrucci, G. A.: Soft ionization chemical analysis of secondary organic aerosol  
589 from green leaf volatiles emitted by turf grass, Environ. Sci. Technol., 48, 4835-4843,  
590 10.1021/es405355d, 2014.

591 Jokinen, T., Sipila, M., Richters, S., Kerminen, V. M., Paasonen, P., Stratmann, F., Worsnop, D., Kulmala,  
592 M., Ehn, M., Herrmann, H., and Berndt, T.: Rapid autoxidation forms highly oxidized RO<sub>2</sub> radicals in  
593 the atmosphere, Angew. Chem. Int. Ed. Engl., 53, 14596-14600, 10.1002/anie.201408566, 2014.

594 Konig, G., Brunda, M., Puxbaum, H., Hewitt, C. N., Duckham, S. C., and Rudolph, J.: Relative  
595 contribution of oxygenated hydrocarbons to the total biogenic voc emissions of selected mid-european  
596 agricultural and natural plant-species, Atmos. Environ., 29, 861-874, Doi 10.1016/1352-2310(95)00026-  
597 U, 1995.

598 Kristensen, K., Cui, T., Zhang, H., Gold, A., Glasius, M., and Surratt, J. D.: Dimers in alpha-pinene  
599 secondary organic aerosol: effect of hydroxyl radical, ozone, relative humidity and aerosol acidity, Atmos.  
600 Chem. Phys., 14, 4201-4218, 10.5194/acp-14-4201-2014, 2014.



601 Kurten, T., Rissanen, M. P., Mackeprang, K., Thornton, J. A., Hyttinen, N., Jorgensen, S., Ehn, M., and  
602 Kjaergaard, H. G.: Computational study of hydrogen shifts and ring-opening mechanisms in alpha-pinene  
603 ozonolysis products, *J. Phys. Chem. A*, 119, 11366-11375, 10.1021/acs.jpca.5b08948, 2015.

604 Lambe, A. T., Onasch, T. B., Massoli, P., Croasdale, D. R., Wright, J. P., Ahern, A. T., Williams, L. R.,  
605 Worsnop, D. R., Brune, W. H., and Davidovits, P.: Laboratory studies of the chemical composition and  
606 cloud condensation nuclei (CCN) activity of secondary organic aerosol (SOA) and oxidized primary  
607 organic aerosol (OPOA), *Atmos. Chem. Phys.*, 11, 8913-8928, 10.5194/acp-11-8913-2011, 2011.

608 Lambe, A. T., Onasch, T. B., Croasdale, D. R., Wright, J. P., Martin, A. T., Franklin, J. P., Massoli, P.,  
609 Kroll, J. H., Canagaratna, M. R., Brune, W. H., Worsnop, D. R., and Davidovits, P.: Transitions from  
610 functionalization to fragmentation reactions of laboratory secondary organic aerosol (SOA) generated  
611 from the OH oxidation of alkane precursors, *Environ. Sci. Technol.*, 46, 5430-5437, 10.1021/es300274t,  
612 2012.

613 Li, K., Liggio, J., Lee, P., Han, C., Liu, Q. F., and Li, S. M.: Secondary organic aerosol formation from  
614 alpha-pinene, alkanes, and oil-sands-related precursors in a new oxidation flow reactor, *Atmos. Chem.*  
615 *Phys.*, 19, 9715-9731, 10.5194/acp-19-9715-2019, 2019.

616 Lin, Y. H., Zhang, Z. F., Docherty, K. S., Zhang, H. F., Budisulistiorini, S. H., Rubitschun, C. L., Shaw,  
617 S. L., Knipping, E. M., Edgerton, E. S., Kleindienst, T. E., Gold, A., and Surratt, J. D.: Isoprene  
618 epoxydiols as precursors to secondary organic aerosol formation: acid-catalyzed reactive uptake studies  
619 with authentic compounds, *Environ. Sci. Technol.*, 46, 250-258, 10.1021/es202554c, 2012.

620 Lin, Y. H., Knipping, E. M., Edgerton, E. S., Shaw, S. L., and Surratt, J. D.: Investigating the influences  
621 of SO<sub>2</sub> and NH<sub>3</sub> levels on isoprene-derived secondary organic aerosol formation using conditional  
622 sampling approaches, *Atmos. Chem. Phys.*, 13, 8457-8470, 10.5194/acp-13-8457-2013, 2013.

623 Liu, C. G., Chen, T. Z., Liu, Y. C., Liu, J., He, H., and Zhang, P.: Enhancement of secondary organic  
624 aerosol formation and its oxidation state by SO<sub>2</sub> during photooxidation of 2-methoxyphenol, *Atmos.*  
625 *Chem. Phys.*, 19, 2687-2700, 10.5194/acp-19-2687-2019, 2019a.

626 Liu, C. G., Liu, Y. C., Chen, T. Z., Liu, J., and He, H.: Rate constant and secondary organic aerosol  
627 formation from the gas-phase reaction of eugenol with hydroxyl radicals, *Atmos. Chem. Phys.*, 19, 2001-  
628 2013, 10.5194/acp-19-2001-2019, 2019b.

629 Liu, S. J., Jia, L., Xu, Y. F., Tsona, N. T., Ge, S. S., and Du, L.: Photooxidation of cyclohexene in the

630 presence of SO<sub>2</sub>: SOA yield and chemical composition, *Atmos. Chem. Phys.*, 17, 13329-13343,  
631 10.5194/acp-17-13329-2017, 2017.

632 Mackenzie-Rae, F. A., Wallis, H. J., Rickard, A. R., Pereira, K. L., Saunders, S. M., Wang, X. M., and  
633 Hamilton, J. F.: Ozonolysis of alpha-phellandrene - Part 2: Compositional analysis of secondary organic  
634 aerosol highlights the role of stabilised Criegee intermediates, *Atmos. Chem. Phys.*, 18, 4673-4693,  
635 10.5194/acp-18-4673-2018, 2018.

636 McFiggans, G., Mentel, T. F., Wildt, J., Pullinen, I., Kang, S., Kleist, E., Schmitt, S., Springer, M.,  
637 Tillmann, R., Wu, C., Zhao, D., Hallquist, M., Faxon, C., Le Breton, M., Hallquist, A. M., Simpson, D.,  
638 Bergstrom, R., Jenkin, M. E., Ehn, M., Thornton, J. A., Alfarra, M. R., Bannan, T. J., Percival, C. J.,  
639 Priestley, M., Topping, D., and Kiendler-Scharr, A.: Secondary organic aerosol reduced by mixture of  
640 atmospheric vapours, *Nature*, 565, 587-593, 10.1038/s41586-018-0871-y, 2019.

641 Newland, M. J., Rickard, A. R., Alam, M. S., Vereecken, L., Munoz, A., Rodenas, M., and Bloss, W. J.:  
642 Kinetics of stabilised Criegee intermediates derived from alkene ozonolysis: reactions with SO<sub>2</sub>, H<sub>2</sub>O  
643 and decomposition under boundary layer conditions, *Phys. Chem. Chem. Phys.*, 17, 4076-4088,  
644 10.1039/c4cp04186k, 2015a.

645 Newland, M. J., Rickard, A. R., Vereecken, L., Munoz, A., Rodenas, M., and Bloss, W. J.: Atmospheric  
646 isoprene ozonolysis: impacts of stabilised Criegee intermediate reactions with SO<sub>2</sub>, H<sub>2</sub>O and dimethyl  
647 sulfide, *Atmos. Chem. Phys.*, 15, 9521-9536, 10.5194/acp-15-9521-2015, 2015b.

648 Newland, M. J., Rickard, A. R., Sherwen, T., Evans, M. J., Vereecken, L., Munoz, A., Rodenas, M., and  
649 Bloss, W. J.: The atmospheric impacts of monoterpene ozonolysis on global stabilised Criegee  
650 intermediate budgets and SO<sub>2</sub> oxidation: experiment, theory and modelling, *Atmos. Chem. Phys.*, 18,  
651 6095-6120, 10.5194/acp-18-6095-2018, 2018.

652 Ng, N. L., Canagaratna, M. R., Jimenez, J. L., Chhabra, P. S., Seinfeld, J. H., and Worsnop, D. R.:  
653 Changes in organic aerosol composition with aging inferred from aerosol mass spectra, *Atmos. Chem.*  
654 *Phys.*, 11, 6465-6474, 10.5194/acp-11-6465-2011, 2011.

655 Offenberg, J. H., Lewandowski, M., Edney, E. O., Kleindienst, T. E., and Jaoui, M.: Influence of aerosol  
656 acidity on the formation of secondary organic aerosol from biogenic precursor hydrocarbons, *Environ.*  
657 *Sci. Technol.*, 43, 7742-7747, 10.1021/es901538e, 2009.

658 Pankow, J. F., Luo, W. T., Bender, D. A., Isabelle, L. M., Hollingsworth, J. S., Chen, C., Asher, W. E.,

659 and Zogorski, J. S.: Concentrations and co-occurrence correlations of 88 volatile organic compounds  
660 (VOCs) in the ambient air of 13 semi-rural to urban locations in the United States, *Atmos. Environ.*, 37,  
661 5023-5046, 10.1016/j.atmosenv.2003.08.006, 2003.

662 Peng, X., Vasilakos, P., Nenes, A., Shi, G., Qian, Y., Shi, X., Xiao, Z., Chen, K., Feng, Y., and Russell,  
663 A. G.: Detailed analysis of estimated ph, activity coefficients, and ion concentrations between the three  
664 aerosol thermodynamic models, *Environ. Sci. Technol.*, 53, 8903-8913, 10.1021/acs.est.9b00181, 2019.

665 Ren, Y. G., Cai, M., Daele, V., and Mellouki, A.: Rate coefficients for the reactions of OH radical and  
666 ozone with a series of unsaturated esters, *Atmos. Environ.*, 200, 243-253,  
667 10.1016/j.atmosenv.2018.12.017, 2019.

668 Riva, M., Bell, D. M., Hansen, A. M., Drozd, G. T., Zhang, Z., Gold, A., Imre, D., Surratt, J. D., Glasius,  
669 M., and Zelenyuk, A.: Effect of organic coatings, humidity and aerosol acidity on multiphase chemistry  
670 of isoprene epoxydiols, *Environ. Sci. Technol.*, 50, 5580-5588, 10.1021/acs.est.5b06050, 2016.

671 Rivela, C. B., Blanco, M. B., and Teruel, M. A.: Atmospheric degradation of industrial fluorinated  
672 acrylates and methacrylates with Cl atoms at atmospheric pressure and 298 K, *Atmos. Environ.*, 178,  
673 206-213, 10.1016/j.atmosenv.2018.01.055, 2018.

674 Rodigast, M., Mutzel, A., and Herrmann, H.: A quantification method for heat-decomposable  
675 methylglyoxal oligomers and its application on 1,3,5-trimethylbenzene SOA, *Atmos. Chem. Phys.*, 17,  
676 3929-3943, 10.5194/acp-17-3929-2017, 2017.

677 Sadezky, A., Chaimbault, P., Mellouki, A., Rompp, A., Winterhalter, R., Le Bras, G., and Moortgat, G.  
678 K.: Formation of secondary organic aerosol and oligomers from the ozonolysis of enol ethers, *Atmos.*  
679 *Chem. Phys.*, 6, 5009-5024, DOI 10.5194/acp-6-5009-2006, 2006.

680 Sadezky, A., Winterhalter, R., Kanawati, B., Rompp, A., Spengler, B., Mellouki, A., Le Bras, G.,  
681 Chaimbault, P., and Moortgat, G. K.: Oligomer formation during gas-phase ozonolysis of small alkenes  
682 and enol ethers: new evidence for the central role of the Criegee Intermediate as oligomer chain unit,  
683 *Atmos. Chem. Phys.*, 8, 2667-2699, DOI 10.5194/acp-8-2667-2008, 2008.

684 Salgado, M. S., Gallego-Iniesta, M. P., Martin, M. P., Tapia, A., and Cabanas, B.: Night-time atmospheric  
685 chemistry of methacrylates, *Environ. Sci. Pollut. Res. Int.*, 18, 940-948, 10.1007/s11356-011-0448-x,  
686 2011.

687 Shu, Y. J., Ji, J., Xu, Y., Deng, J. G., Huang, H. B., He, M., Leung, D. Y. C., Wu, M. Y., Liu, S. W., Liu,

688 S. L., Liu, G. Y., Xie, R. J., Feng, Q. Y., Zhan, Y. J., Fang, R. M., and Ye, X. G.: Promotional role of Mn  
689 doping on catalytic oxidation of VOCs over mesoporous TiO<sub>2</sub> under vacuum ultraviolet (VUV)  
690 irradiation, *Appl. Catal. B-Environ.*, 220, 78-87, 10.1016/j.apcatb.2017.08.019, 2018.

691 Sun, Y., Zhang, Q., Hu, J., Chen, J., and Wang, W.: Theoretical study for OH radical-initiated atmospheric  
692 oxidation of ethyl acrylate, *Chemosphere*, 119, 626-633, 10.1016/j.chemosphere.2014.07.056, 2015.

693 Surratt, J. D., Chan, A. W., Eddingsaas, N. C., Chan, M., Loza, C. L., Kwan, A. J., Hersey, S. P., Flagan,  
694 R. C., Wennberg, P. O., and Seinfeld, J. H.: Reactive intermediates revealed in secondary organic aerosol  
695 formation from isoprene, *Proc. Natl. Acad. Sci. USA.*, 107, 6640-6645, 10.1073/pnas.0911114107, 2010.

696 Taccone, R. A., Moreno, A., Colmenar, I., Salgado, S., Martin, M. P., and Cabanas, B.: Kinetic study of  
697 the OH, NO<sub>3</sub> radicals and Cl atom initiated atmospheric photo-oxidation of Iso-propenyl methyl ether,  
698 *Atmos. Environ.*, 127, 80-89, 10.1016/j.atmosenv.2015.12.033, 2016.

699 Teruel, M. A., Lopez, R. S. P., Barnes, I., and Blanco, M. B.: Night-time atmospheric degradation of a  
700 series of butyl methacrylates, *Chem. Phys. Lett.*, 664, 205-212, 10.1016/j.cplett.2016.09.040, 2016.

701 Ulbrich, I. M., Canagaratna, M. R., Zhang, Q., Worsnop, D. R., and Jimenez, J. L.: Interpretation of  
702 organic components from Positive Matrix Factorization of aerosol mass spectrometric data, *Atmos.*  
703 *Chem. Phys.*, 9, 2891-2918, 10.5194/acp-9-2891-2009, 2009.

704 Vereecken, L., and Francisco, J. S.: Theoretical studies of atmospheric reaction mechanisms in the  
705 troposphere, *Chem. Soc. Rev.*, 41, 6259-6293, 10.1039/c2cs35070j, 2012.

706 Wang, K., Ge, M. F., and Wang, W. G.: Kinetics of the gas-phase reactions of NO<sub>3</sub> radicals with ethyl  
707 acrylate, n-butyl acrylate, methyl methacrylate and ethyl methacrylate, *Atmos. Environ.*, 44, 1847-1850,  
708 10.1016/j.atmosenv.2010.02.039, 2010.

709 Wong, J. P., Lee, A. K., and Abbatt, J. P.: Impacts of sulfate seed acidity and water content on isoprene  
710 secondary organic aerosol formation, *Environ. Sci. Technol.*, 49, 13215-13221, 10.1021/acs.est.5b02686,  
711 2015.

712 Zhang, P., Chen, T., Liu, J., Liu, C., Ma, J., Ma, Q., Chu, B., and He, H.: Impacts of SO<sub>2</sub>, Relative  
713 humidity, and seed acidity on secondary organic aerosol formation in the ozonolysis of butyl vinyl ether,  
714 *Environ. Sci. Technol.*, 53, 8845-8853, 10.1021/acs.est.9b02702, 2019.

715 Zhang, P., Chen, T., Liu, J., Chu, B., Ma, Q., Ma, J., and He, H.: Impacts of mixed gaseous and particulate  
716 pollutants on secondary particle formation during ozonolysis of butyl vinyl ether, *Environ. Sci. Technol.*,

717 54, 3909-3919, 10.1021/acs.est.9b07650, 2020.

718 Zhang, Q., Alfarra, M. R., Worsnop, D. R., Allan, J. D., Coe, H., Canagaratna, M. R., and Jimenez, J. L.:

719 Deconvolution and quantification of hydrocarbon-like and oxygenated organic aerosols based on aerosol

720 mass spectrometry, *Environ. Sci. Technol.*, 39, 4938-4952, 10.1021/es048568l, 2005.

721 Zhang, X., Cappa, C. D., Jathar, S. H., McVay, R. C., Ensberg, J. J., Kleeman, M. J., and Seinfeld, J. H.:

722 Influence of vapor wall loss in laboratory chambers on yields of secondary organic aerosol, *Proc. Natl.*

723 *Acad. Sci. USA.*, 111, 5802-5807, 10.1073/pnas.1404727111, 2014.

724 Zhao, D. F., Schmitt, S. H., Wang, M. J., Acir, I. H., Tillmann, R., Tan, Z. F., Novelli, A., Fuchs, H.,

725 Pullinen, I., Wegener, R., Rohrer, F., Wildt, J., Kiendler-Scharr, A., Wahner, A., and Mentel, T. F.: Effects

726 of NO<sub>x</sub> and SO<sub>2</sub> on the secondary organic aerosol formation from photooxidation of alpha-pinene and

727 limonene, *Atmos. Chem. Phys.*, 18, 1611-1628, 10.5194/acp-18-1611-2018, 2018.

728 Zhao, Y., Wingen, L. M., Perraud, V., Greaves, J., and Finlayson-Pitts, B. J.: Role of the reaction of

729 stabilized Criegee intermediates with peroxy radicals in particle formation and growth in air, *Phys. Chem.*

730 *Chem. Phys.*, 17, 12500-12514, 10.1039/c5cp01171j, 2015.

731